https://doi.org/10.5194/egusphere-2026-224
Preprint. Discussion started: 5 March 2026

Comparison of two oxidation flow reactors for measuring aged aerosol from passenger car exhaust

Katariina Kylämäki[1], Milja Jäppi[1], Leïla Simon[2,*], Wojciech Honkisz[3], Petteri Marjanen[1], Laura Salo[1], Teemu Lepistö[1], Henna Lintusaari[1], Luis Barreira[2], Hannu Kuutti[4], Matti Rissanen[1,5], Piotr Bielaczyc[3,¤], Hilkka Timonen[2], Päivi Aakko-Saksa[4], Topi Rönkkö[1]

[1]Aerosol Physics Laboratory, Physics Unit, Tampere University, 33720 Tampere, Finland

[2]Atmospheric Composition research, Finnish Meteorological Institute, 00560 Helsinki, Finland

[3]BOSMAL Automotive Research and Development Institute Ltd, 43-300 Bielsko-Biała, Poland

[4]VTT Technical Research Centre of Finland Ltd, 02150 Espoo, Finland

[5]Department of Chemistry, University of Helsinki, 00560 Helsinki, Finland

*Now at: PSI Center for Energy and Environmental Sciences, 5232 Villigen PSI, Switzerland

[¤]Now at: Cracow University of Technology, 31-155 Cracow, Poland

Correspondence to: Katariina Kylämäki (katariina.kylamaki@tuni.fi) and Topi Rönkkö (topi.ronkko@tuni.fi)

Abstract

Oxidation flow reactors (OFRs) are a practical way to assess the secondary aerosol (SecA) mass formation potential of any gas mixture of interest in relatively short processing timescales. In this study, two OFRs were assembled in parallel and used to investigate the photochemical aging and formation of secondary aerosol from exhaust emissions of seven passenger cars. The potential aerosol mass OFR (PAM-OFR) and the Dekati OFR (DOFR) have differences in reactor volume, wall material, residence time and ultraviolet (UV) wavelengths, but the particle number and mass size distributions measured after them were comparable when averaged over the transient driving cycle. The average secondary particle mass emission factor (EF) for all 34 cycles was 22.90 mg km^{-1} for the PAM-OFR and 15.77 mg km^{-1} for the DOFR. The fuel and exhaust after-treatment technology affected the difference between the PAM-OFR and the DOFR EFs. With gasoline cars, fast bursts of SecA formation during cold start and highway driving were captured more clearly by the DOFR, which led to DOFR EFs exceeding PAM-OFR EFs. However, with modern diesel cars, the CNG car or hybrid cars that all produced low fresh PM emissions, the SecA mass EFs were higher from the PAM-OFR than from the DOFR. OH exposure did not cause the differences in emission factors between the OFRs, because the OH exposure range was small. Background SecA formation from the PAM-OFR was visible in the particle size distributions of the cleanest cars, which was corrected for in the EF calculations. On average, the PAM-OFR produced more background particle mass (9.10 µg m^{-3}) than the DOFR (0.36 µg m^{-3}).

https://doi.org/10.5194/egusphere-2026-224
Preprint. Discussion started: 5 March 2026

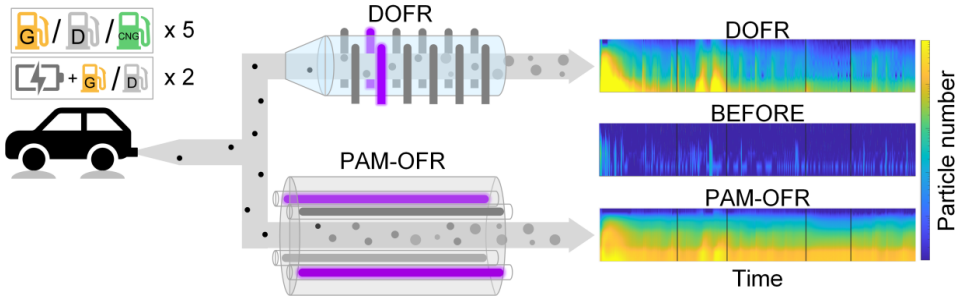

Keywords: Secondary Aerosol, SOA, light-duty vehicles, particle emissions

1 Introduction

Traffic is a source of significant gaseous and particulate emissions: roughly half of total nitrogen oxides (NO_x) and one fifth of total PM2.5 (particulate matter of diameter ≤2.5 µm) emissions in the European Union were estimated to be caused by the transport sector in 2023 (EEA data viewer, 2025). PM2.5 is known to be a major contributor to premature deaths world-wide (Cohen et al. 2017), and vehicle exhaust has been suggested to be a particularly relevant emission source regarding the adverse health effects (Park et al. 2018). In the atmosphere, anthropogenic emissions react with oxidants, mainly hydroxyl (OH) radical. Secondary aerosol (SecA) is formed by the oxidation of gaseous precursors followed by the condensation of oxidation products to particle phase. Daellenbach et al. (2020) found that anthropogenic secondary organic aerosol (SOA) is the most important contributor to aerosol oxidative potential in most parts of Europe, highlighting the importance of understanding the SecA formation processes and sources. Photochemical aging of vehicle exhaust has been found to greatly increase the particle mass (Alanen et al., 2017; Gordon et al., 2014b; Karjalainen et al., 2019; Simonen et al., 2019; Watne et al., 2018) and to cause significant cytotoxicity and DNA damage to bronchial epithelial cells (Delaval et al., 2025).

The formation of secondary aerosol is a complex process. Volatile organic compounds (VOC), sulfur oxides (SO_x), NO_x and ammonia (NH_3) have been identified as major precursors to SecA in exhaust emissions, but a comprehensive understanding of the photochemical reactions and particle formation mechanisms is still lacking. Smog chambers, enclosing volumes of several m^3, have been essential in simulating atmospheric chemistry (Lee et al., 2009). In emission and air quality measurements, the use of oxidation flow reactors (OFR) has increased over smog chambers, because the OFRs were designed to be easier to transport, have lower wall losses and shorter exposure times (Zhang et al., 2024). An OFR is a flow reactor using substantially higher oxidant concentrations than in the atmosphere, so a photochemical age of multiple days can be achieved in minutes (Peng & Jimenez, 2020).

OFRs have been used to investigate the effect of fuel (Timonen et al., 2017; Alanen et al., 2017; Watne et al., 2018; Saarikoski et al., 2024), engine technology (Simonen et al., 2019; Zhao et al., 2018; Saarikoski et al., 2024), after-treatment systems (Karjalainen et al., 2019; Pieber et al., 2018; Paul et al., 2024; Jathar et al., 2017) and driving conditions (Zhang et al., 2023; Simonen et al., 2019; Kuittinen et al., 2021; Karjalainen et al., 2016) on SecA formation. The composition of aged particles from gasoline vehicles is generally dominated by ammonium

https://doi.org/10.5194/egusphere-2026-224
Preprint. Discussion started: 5 March 2026

nitrate NH_4NO_3 (Simonen et al., 2019; Kuittinen et al., 2021) whereas Alanen et al. (2017) found that organic matter dominated in aged particles from a natural gas engine. In this article, the term fresh aerosol refers to exhaust that has been diluted and cooled rapidly after emission from the tailpipe, whereas aged aerosol includes both fresh and secondary aerosol. Catalysts and diesel particulate filters (DPFs) are efficient in decreasing fresh and aged particle emissions (Karjalainen et al., 2019; Platt et al., 2017). Timonen et al. (2017) observed that the addition of alcohol to the fuel from 10 to 100% significantly decreased aromatic compounds in the exhaust and thus also SecA formation. For gasoline vehicles, cold start (Simonen et al., 2019; Kuittinen et al., 2021), accelerations and high-speed driving (Zhang et al., 2023; Zhao et al., 2018) have been found to increase SecA formation.

There are many different designs of OFRs. The flow profile, wall material, and surface area to volume ratio influence the wall losses of particles and low-volatility organic compounds (LVOC) (Zhang et al., 2024). If the OH exposure is too high, LVOCs can react with OH more times than realistic in the atmosphere, resulting in fragmentation and thus an increase in volatility (Palm et al., 2016). LVOC losses on walls and by fragmentation lead to a smaller fraction of LVOCs condensed on aerosol particles and therefore an underestimation of the potential SecA mass produced. The condensation rate of LVOCs on aerosol particles is dependent on particle number, which is affected by dilution of the sample. Tkacik et al. (2014) observed that the photochemical age, used in parallel with OH exposure to describe the stage of oxidation in the OFR, greatly affects the SecA mass concentration and composition. Even though OH exposure and photochemical age are critical for the interpretation of the results, not all OFR studies report the values or the calculation methods clearly. With transient vehicle emissions, changes in OH exposure during the measurements are inevitable, which introduces uncertainty to the results.

OFR comparison measurements in real applications are still scarce. While smog chambers have been compared with different OFR systems (Pieber et al., 2018; Li et al., 2024; Ihalainen et al., 2018; Lambe et al., 2015), OFRs have been compared with each other mostly in terms of particle wall losses, residence time distributions (RTD) and SOA yields (Lambe et al., 2011; Li et al., 2019; Xu et al., 2021; Wu et al., 2023; Ihalainen et al., 2018; Simonen et al., 2017). Bruns et al. (2015) compared two OFRs, a potential aerosol mass (PAM) OFR and a micro smog chamber (MSC), with a smog chamber in wood combustion experiment. They found that while the PAM-OFR agreed with smog chamber in terms of emission factors and particle chemical composition, the MSC produced lower emission factors. Simonen et al. (2024) used semi-synthetic vehicle emission data to compare a PAM-OFR and a prototype Dekati OFR (DOFR). They calculated a reference SOA time series using hydrocarbon concentration from a gasoline vehicle and then convolved that with the OFR transfer functions. The conclusion was that the PAM-OFR tended to overestimate SOA production factors compared to reference SOA especially with shorter segments of the driving cycle, and that the production factor calculation method affected the errors with both OFRs. The findings of the studies mentioned indicate that comparing results quantitatively from different OFR studies can be challenging and unreliable. Hence, understanding the differences between OFRs is necessary to accurately evaluate emission mitigation approaches to reduce SecA formation and adverse health effects.

The aim of this study was to compare the particle size distributions and emission factors produced by two differently designed OFRs in a realistic application: a PAM-OFR and a DOFR were used in parallel in a chassis dynamometer measurement campaign. While both OFRs utilize OH radical chemistry in SecA formation, the

https://doi.org/10.5194/egusphere-2026-224
Preprint. Discussion started: 5 March 2026

ozone necessary for OH radical formation is generated inside the PAM-OFR, whereas the DOFR uses an external ozone generator. In addition, the DOFR has a smaller volume and thus a narrower residence time distribution than the PAM-OFR. Exhaust emissions from seven passenger cars of varying emission classes (Euro 4 to Euro 6d), including gasoline, diesel, compressed natural gas (CNG) and plug-in hybrid electric vehicles (PHEVs), were measured on a chassis dynamometer, and the gas and particle phase of the exhaust was characterized. The extensive experimental setup included high time resolution measurement of the particle size distribution before and after the OFRs and aged particle chemical composition measurement.

2 Materials and methods

Seven passenger cars with various engine and exhaust after-treatment technologies were chosen for the measurements (Table 1). The vehicles were measured in a temperature-controlled test cell (WK 643; Weiss Technik, Germany) on a chassis dynamometer (Zoellner 48" 4WD; AVL, Austria). Each car was measured at three temperatures: -9 ˚C, +23 ˚C, and +35˚C. The gasoline and diesel fuels used in the study were provided by BOSMAL and VTT and met the European standards for gasoline (EN228) and automotive diesel (EN590), and the CNG was from the Finnish natural gas pipeline. The CNG car operated primarily on CNG, but used gasoline in certain conditions, such as during start-up and heavy driving, as specified by the manufacturer.

Table 1. Vehicle information, including specifications of the exhaust after-treatment system (EAS)

Name	Model year	Mileage (km)	Fuel	Engine	Euro class	EAS
PHEV-G- Euro 6d	2022	16 000	Gasoline PHEV	1.6 L GDI	6d	TWC, GPF
PHEV-D-Euro 6d	2020	23 000	Diesel PHEV	2.0 L DI	6d	DOC, SCR, DPF
G-Euro 6d	2023	4 000	Gasoline	1.0 L GDI	6d	TWC, GPF
D-Euro 6d	2022	12 000	Diesel	1.5 L DI	6d	DOC, SCR, DPF
G-Euro 6b	2015	110 000	Gasoline	2.0 L GCI	6b	TWC
D-Euro 4	2006	232 000	Diesel	2.2 L CI	4	DOC
CNG-Euro 6d-TEMP	2020	39 000	CNG*	1.5 L GDI	6d-TEMP	TWC

GDI = gasoline direct injection, DI = (diesel) direct injection, CI = compression ignition, TWC = three-way catalyst, GPF = gasoline particulate filter, DOC = diesel oxidation catalyst, SCR = selective catalytic reduction, DPF = diesel particulate filter
*CNG car used gasoline as a back-up fuel

The measurement cycle was built based on real driving route measurements conducted on the road near the laboratory facilities. The real driving route consisted of 35 minutes of urban, 13 minutes of highway and 14 minutes of rural driving. The vehicle was parked for 10 minutes in the middle of the route to measure a warm start. The maximum speed during the cycle was 146 km/h and the average speed without parking was 46 km/h. The speed profile (see Fig. 4a) of the route was programmed into the chassis dynamometer, allowing the measurement conditions, such as temperature, to be controlled. Certain boundary conditions, such as temperatures, were chosen in accordance with the expected Euro 7 standard. The cycle duration was 72 min, which covered a distance of approximately 47 km. The vehicles were mounted on a chassis dynamometer without starting the engine, so that all measured cycles began with a cold start.

https://doi.org/10.5194/egusphere-2026-224
Preprint. Discussion started: 5 March 2026

The schematic of the instrumentation is presented in Fig. 1. Part of the exhaust gas flow was led into another room that was kept at normal room temperature for the measurement equipment through a stainless-steel line (length 5.5 m) heated to 300˚C. The exhaust gas was drawn into a porous tube diluter (PTD), followed by a residence time tube (RTT). Then, the sample was split into two lines: one line included the studied OFRs, and the other line was used to measure the sample without photochemical aging, referred to as fresh aerosol. Aged aerosol refers to the aerosol measured after the OFRs, including both fresh and secondary aerosol. Ejector diluters (EDs; Dekati, Finland) were employed in both fresh and aged lines, and they were chosen to stabilize the flows in the PTD, as the outlet of an ED is at room pressure. The dilution air used in the measurements was cleaned of particles, oil, CO_2 and other gaseous substances using adsorption-based filters (K-MT 6-LAB and 75-62 FT-IR Purge Gas Generator; Parker, USA). The same dilution air was used in background measurements in between measurement cycles.

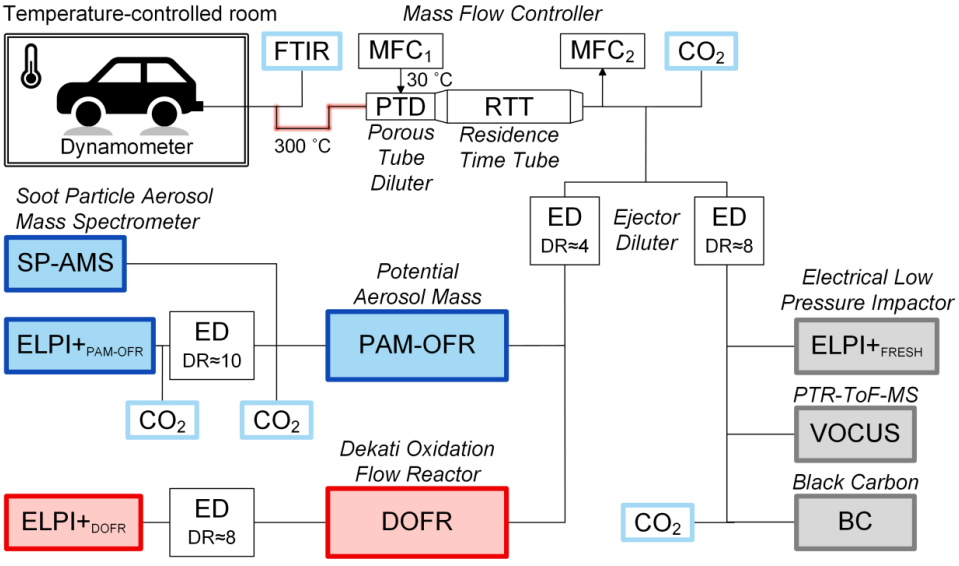

Figure 1. Schematic of the aerosol instrumentation

The dilution ratios (DRs) were calculated based on the carbon dioxide (CO_2) concentrations measured by LI-840A, LI-850 (LI-COR, USA) and Sidor (SICK Maihak, Germany) instruments. Raw CO_2 was measured with a Fourier transform infrared (FTIR) analyzer (BOB-1000; A&D Technology, Japan). The DR of the PTD was adjusted by driving at a constant speed of 80 km/h after the actual measurement cycle, so that the CO_2 levels remained stable, and the DR determination did not affect the cold start. The DR of the PTD was always adjusted to approx. 12, which has been found to best imitate the nanoparticle formation processes during dilution and cooling of the exhaust gas after exiting the exhaust pipe (Rönkkö et al., 2006; Keskinen and Rönkkö, 2010).

2.1 Oxidation flow reactors

The potential aerosol mass OFR (PAM-OFR; Aerodyne Research, USA), developed by Kang et al. (2007) and commercialized by Aerodyne Research (US), was a 13.3 L aluminum-walled reactor (Fig. 2a). There were four low-pressure Hg-lamps inside the reactor, of which two 185 nm UV lamps were used in the measurements. One

https://doi.org/10.5194/egusphere-2026-224
Preprint. Discussion started: 5 March 2026

of the lamps was partially covered to reduce UV intensity in the OFR. To prevent overheating and oxidation product buildup on the lamp surfaces, the lamps were protected with a nitrogen flow around them in quartz sleeves. The voltage across the lamps was set to 2.8 V, out of the maximum of 10 V. The PAM-OFR was used in OFR185 mode, according to Li et al. (2015) terminology, in which ozone (O_3) is generated inside the OFR from the photolysis of O_2 at 185 nm. O_3 undergoes photolysis at 254 nm to produce OH. To get the water necessary for the formation of OH radicals, compressed air humidified with a bubbler was mixed into the sample flow before the reactor. The relative humidity (RH) inside the PAM-OFR during the experiments was on average (44.0±2.1) % and the reactor flow was 8.6 lpm.

The Dekati OFR (DOFR; Dekati, Finland) was used parallel to the PAM-OFR. The DOFR (Fig. 2b) has a similar design to the Tampere secondary aerosol reactor (TSAR), which was developed to measure vehicle emissions in transient driving by Simonen et al. (2017). Compared to the PAM-OFR, the DOFR quartz glass reactor was smaller in size (approx. 3.3 L) and had a conical inlet. Two or three of the twelve 254 nm UV lamps were used for the measurements, so the DOFR is classified as an OFR254. In the DOFR setup, the lamps were positioned just outside the reactor, whereas in the PAM-OFR, they were placed inside the aluminum reactor. The DOFR has a separate O_3 generator. The RH inside the DOFR was on average (26.2±5.4) %, and the humidity was created with a similar bubbler than for the PAM-OFR. The flows in the DOFR were changed in the middle of the campaign: Reactor flow was decreased from 8.8 to 6.0 lpm and inlet flow from 3.5 to 2.3 lpm by increasing the DR of the ED after the OFR. Two UV lamps instead of previous three were used to achieve the same OH exposure, and the primary DR and RH stayed the same. The residence time in the DOFR increased slightly, however, this change was not expected to significantly influence the chemical processes, since the OH exposure was adjusted to be similar. Additionally, the DRs were corrected on a cycle-by-cycle basis.

https://doi.org/10.5194/egusphere-2026-224
Preprint. Discussion started: 5 March 2026

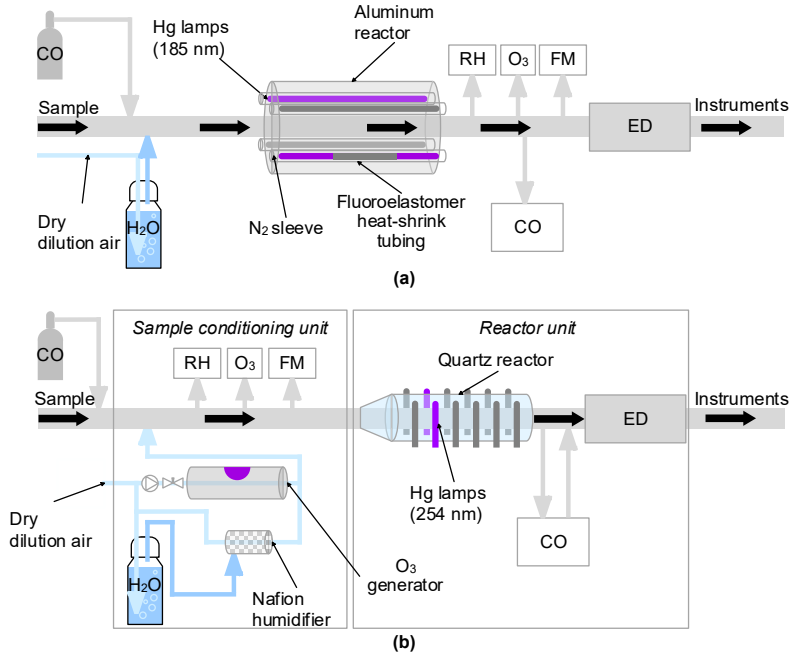

Figure 2. Detailed schematics of a) the Potential Aerosol Mass (PAM) OFR (Aerodyne Research, US) and b) the Dekati OFR (DOFR; Dekati Ltd. FI). Relative humidity (RH), ozone (O_3), flow (flow meter, FM) and carbon monoxide (CO) were measured to determine the aging conditions.

To reduce the background SecA concentrations, the OFRs were cleaned daily during the campaign, sometimes in the beginning and end of the measurement day. The cleaning was performed by setting the lamp voltage to 10 V in the PAM-OFR and by turning all lights on and elevating ozone concentration from 30 ppm to 90 ppm in the DOFR. The cleaning continued until background particle mass (PM) concentrations had stabilized: this took 8-49 minutes (mean 23 min 50 s) in the PAM-OFR and 3-27 minutes (mean 11 min 37 s) in the DOFR. The PAM-OFR surfaces were cleaned manually before the measurement campaign, and the DOFR came straight from the manufacturer. During background measurements, the UV lights were on in their normal setting, but the first and the last background measurements of the day were also performed without the UV lights.

The progress of the oxidation reactions in the OFR is described by exposure to OH radicals. During the background measurements, the OH exposure was monitored and adjusted by measuring CO decay, given by

$$OH_{exp} = \frac{1}{k_{OH+CO}} \ln\left(\frac{[CO]_i}{[CO]_f}\right) \quad (1)$$

where reaction rate constant $k_{OH+CO} = 2.37 \times 10^{-13}$ cm^3 molec.$^{-1}$ s^{-1} (Fiore et al., 2024) and $[CO]_i$ and $[CO]_f$ are the initial and final CO concentrations. After the campaign, the OH exposure was modeled with a 60 s interval using the PAM Chem model (PAM users manual, 2025). The inputs of the model were CO and NO_x concentrations, OH reactivity, RH and temperature of the sample, and photon flux. CO and NO_x concentrations

https://doi.org/10.5194/egusphere-2026-224
Preprint. Discussion started: 5 March 2026

were measured with the FTIR and divided with appropriate DR, and the tracer CO concentration was added to the CO measured by the FTIR. The OH reactivity was calculated based on the concentrations of toluene, xylene and trimethylbenzene, measured by a proton transfer reaction (PTR) mass spectrometer, and their reaction rates with OH (Shaw et al.,2020). The model does not consider the reactions of individual VOCs, but their contribution is estimated with a SO_2 concentration producing the same OH reactivity. The three VOCs were chosen for the calculation because they are important SOA precursors (see e.g. Paul et al., 2024) and their signals can be accurately converted to concentration because they are included in the calibration gas mixture of the PTR. The photon flux was estimated by reproducing the CO decay measurements with the model. The OH exposure was then converted to photochemical age equivalent to time spent in the atmosphere using mean OH concentration in the atmosphere (1.5×10^6 molec. cm^{-3}; Mao et al., 2009) and 24 h d^{-1}. Average photochemical age was (3.52 ± 0.73) d for the PAM-OFR and (3.32 ± 0.65) d for the DOFR over the whole campaign.

The residence time distributions (RTD) of the OFRs were calculated using Eq. S1 and plotted in Fig. S1, using parameters and functions by Simonen et al. (2024). Even though the peaks of the distributions are relatively close to each other (35 s for the PAM-OFR and 27 s for the DOFR), the RTD of the DOFR is narrower (standard deviation σ = 20.81 s) than that of the PAM-OFR (σ = 73.26 s). The mean residence time in DOFR is 41 s and in PAM-OFR 115 s. The LVOC fate was modeled with Palm et al. (2016) model (Fig. S2).

2.2 Aerosol instruments

The particle size distributions of both fresh and aged exhaust aerosol were measured with an electrical low pressure impactor (ELPI+; Dekati, Finland; Keskinen et al., 1992; Järvinen et al., 2014). The measurement principle of the ELPI+ is to charge the particles with a unipolar corona charger, then classify them in a low pressure cascade impactor and detect them with electrometers. Three ELPI+ instruments were used in the measurements, and they were named according to their measurement place; $ELPI+_{fresh}$, $ELPI+_{PAM\text{-}OFR}$ and $ELPI+_{DOFR}$ (see Fig. 1). A comparison measurement between them was performed with room air at the end of the campaign. The comparison measurement revealed a blockage of a nozzle within the $ELPI+_{DOFR}$ impactor, leading to restricted inlet flow, lower speed of the particles and therefore a shift in the impactor cut-off sizes. All three ELPI+ impactors were cleaned at least once during the campaign by washing them in an ultrasonic bath filled with acetone. The blockage was traced to cleaning of the $ELPI+_{DOFR}$ impactor three days before the comparison measurement. The shift was corrected by iterating new cut-off sizes based on the comparison measurement (Fig. S5).

The current distribution of the ELPI+ was converted to particle number and mass size distributions, taking into account the calibration presented by Järvinen et al. (2014) and assuming unit density (1000 kg m^{-3}) for particles. Total particle number and mass were calculated by summing over the distribution. Impactor stages 10-14 were discarded in calculating the total particle mass for the emission factors, because at these stages the currents had a large deviation and negative values. Thus, only particles with a diameter of 6-952 nm were considered for $ELPI+_{FRESH}$, 6-941 nm for $ELPI+_{PAM}$ and 6-947 nm for $ELPI+_{DOFR}$. For total particle number, all stages were used because stages 10-14 have a minimal effect on particle number. Moreover, the particle losses on the OFR walls were corrected for particle mass distributions using transmission efficiencies for PAM-OFR from Karjalainen et al. (2016) and for DOFR from Dekati (Fig. S3). Wall losses were not corrected to particle number distributions to not overestimate potential background of small particles.

https://doi.org/10.5194/egusphere-2026-224
Preprint. Discussion started: 5 March 2026

The composition of aged particles was analyzed with a soot particle aerosol mass spectrometer (SP-AMS; Aerodyne Research, USA). The operation of the SP-AMS is explained more thoroughly in Onasch et al. (2012). Briefly, the aerosol particles are first vaporized with a combination of a laser and a Tungsten vaporizer. Then the fragments are ionized and classified by a time-of-flight (ToF) mass spectrometer. In-depth analysis of the chemical composition and its temporal variation during the driving cycle after the PAM-OFR with the SP-AMS is presented in the article by Simon et al. (2025). The gaseous emissions were measured with the FTIR and a proton transfer reaction PTR-ToF mass spectrometer (Vocus; Tofwerk, Switzerland). In the Vocus, the sample molecules are ionized in PTR with protonated water and classified by time-of-flight (Krechmer et al., 2018). The PTR-ToF was operated at an E/N of 120 Td and calibrated at least twice daily with a 14-component calibration gas mixture. The VOC results will be presented and discussed in a future article. Black carbon (BC) was measured from fresh exhaust with an aethalometer (AE33; Magee Scientific, Slovenia).

The emission factors (EFs) were calculated by multiplying the mass concentrations C_m with exhaust volumetric flow $\dot{Q}_{exh}$ at 0 ˚C, summing over the measurement cycle and dividing with the driven distance s

$$EF = \frac{\sum_i C_{m,i} \dot{Q}_{exh,i} \Delta t_i}{s} \quad (2)$$

to obtain the unit mg km^{-1}. Before using Eq. (2), the mass concentrations were converted to standard temperature (0 ˚C) from the sample temperature of 20 ˚C and average background concentration during background measurement after the cycle was subtracted. The concentrations measured after the OFR are delayed because of the residence time of the OFR and also distorted because of the residence time distribution. The delay was corrected with a simple time shift correction between C_m and $\dot{Q}_{exh}$ for each cycle. A similar correction was done for all concentrations, also before the OFRs, to consider residence times of the sampling lines. The distortion was corrected by convolving $\dot{Q}_{exh}$ and RTD function $E(t)$ as described in Simonen et al. (2024). Secondary EFs were calculated by subtracting fresh EF from aged EF.

3 Results and discussion

3.1 Particle size distributions

Figure 3 shows the average fresh and aged particle size distributions for three vehicles as examples of different vehicle categories: G-Euro 6d (modern), D-Euro 4 (old) and PHEV-D-Euro 6d (PHEV). The average aged particle number (PN) and particle mass (PM) size distributions were comparable for the PAM-OFR and the DOFR. Generally, the particle size distributions of exhaust after the PAM-OFR and the DOFR showed a mode at 10 nm and at 100 nm particle sizes. For the G-Euro 6d car (Fig. 3 a, d), PN and PM concentrations after both OFRs increased three orders of magnitude compared to the fresh exhaust. A large increase was expected based on previous studies (Pieber et al., 2018; Paul et al., 2024). The shapes of the PN and PM size distributions were similar between the OFRs.

The lack of DPF in the D-Euro 4 car (Fig. 3 b, e) caused high PN and PM concentrations in the fresh exhaust. PN or PM concentrations did not increase much with aging but mean particle size increased slightly. Compared to Karjalainen et al. (2019) study done on a heavy-duty engine, we observed a stronger soot mode and no nucleation particles in the fresh exhaust, and therefore no growth of nucleation particles with aging. While they also used the

https://doi.org/10.5194/egusphere-2026-224
Preprint. Discussion started: 5 March 2026

PAM-OFR, the driving cycle, engine design and mileage were different compared to our study. The PN and PM size distributions for the PAM-OFR and DOFR were relatively similar, but there was a clear mode in the smallest particle sizes after the PAM-OFR.

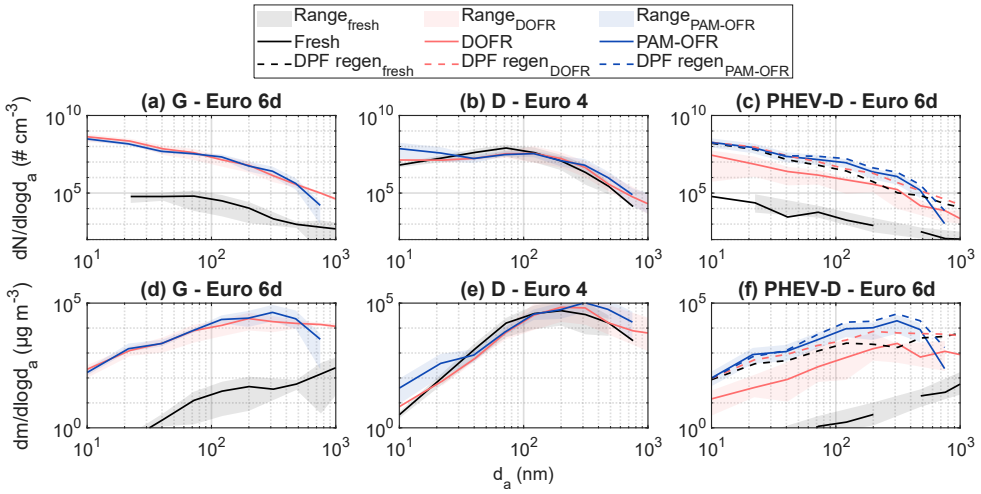

Figure 3. Particle number (a-c) and mass (d-f) size distributions for fresh and aged exhaust. Shaded areas represent the minimum and maximum of all repeated measurements. Results are corrected for DR, standard temperature and particle mass size distributions also for particle losses on OFR walls.

The particle number and mass emissions were very low in the fresh exhaust of the PHEV-D-Euro 6d car because the electric motor was used 69.5 % of the time on average and because the exhaust was treated with a DPF. There was moderate secondary particle formation observed in the OFRs, with higher PN and PM concentrations after the PAM-OFR than the DOFR. During one of the PHEV-D-Euro 6d car cycles (cycle 8 later), there was a DPF regeneration event, so this cycle is separated from the average. The PN_{fresh} and PM_{fresh} emissions increased by three orders of magnitude during DPF regeneration, but aged PN and PM emissions increased by only one order of magnitude. Hartikainen et al. (2023) observed an increase of two orders of magnitude in PM_{fresh} EFs for a Euro 6 diesel car with an internal combustion engine during DPF regeneration. The use of electric motor in the other cycles likely explains the higher contrast in this study.

https://doi.org/10.5194/egusphere-2026-224
Preprint. Discussion started: 5 March 2026

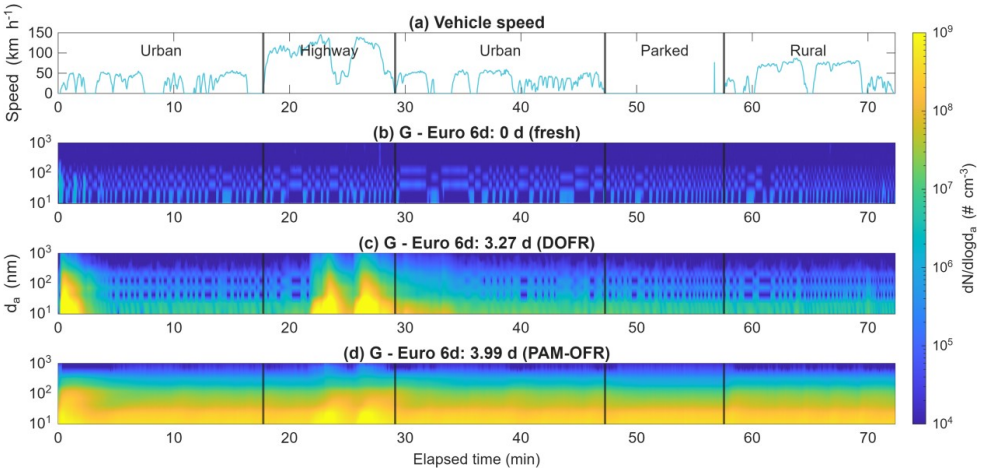

Figure 4. Particle number size distributions (dN/dlogd_a) as a function of time for the Euro 6d gasoline car in fresh exhaust (b) and aged in the DOFR (c) and in the PAM-OFR (d). Distributions were measured with an ambient temperature of +35°C (cycle 14 in Fig. 5 and Table S2) and corrected for DR and standard temperature. Vehicle speed is shown in panel a. Ages correspond to OH exposures of $4.24 \cdot 10^{11}$ molec. cm^{-3} s^{-1} for the DOFR and $5.17 \cdot 10^{11}$ molec. cm^{-3} s^{-1} for the PAM-OFR.

To analyze the effect of transient driving on PM_{aged}, Fig. 4 presents PN size distributions for fresh and aged exhaust for the G-Euro 6d car. Size distributions are shown as a function of time, together with vehicle speed and phases of the driving cycle. For the G-Euro 6d car, the highest SecA production was observed at cold start and during highway driving, which agrees with earlier research results (Hartikainen et al., 2023; Kuittinen et al., 2021; Simonen et al., 2019). While the effect of the cold start and the highway driving was observed after both OFRs, peak concentrations at cold start were roughly an order of magnitude higher after the DOFR than the PAM-OFR.

Particle number time series for the D-Euro 4 and PHEV-D-Euro 6d cars are presented in Fig. S4. For the D-Euro 4 car, all parts of the cycle were relatively similar and cold start did not cause major SecA formation. PAM-OFR and DOFR PN concentrations were on a similar level but again, the changes appeared sharper in the DOFR than in the PAM-OFR. The PAM-OFR and DOFR results were very different for the PHEV-D-Euro 6d car; DOFR PN concentrations increased only at the beginning of the highway part, whereas for PAM-OFR, the PN concentrations were relatively high throughout the cycle. This agrees with the higher average PN distribution of the PAM-OFR compared to the DOFR (Fig. 3c). Both Fig. 4 and Fig. S4 show that the PAM-OFR produced <20 nm particles constantly, even when the vehicles were parked. This is considered background particle formation, and its origin and prevention are discussed more thoroughly in Sect. 3.3.

3.2 Emission factors

Figure 5 presents secondary particle mass emission factors (EFs; mg km^{-1}) of the studied cars for the exhaust aged in the PAM-OFR and the DOFR. The EFs were comparable on average: for all 34 cycles the mean was 22.90 mg km^{-1} for the PAM-OFR and 15.77 mg km^{-1} for the DOFR, while the medians were 18.41 mg km^{-1} and 11.96 mg km^{-1} respectively. However, there were still significant differences in the PAM-OFR and the DOFR EFs: $|EF_{PAM-OFR} - EF_{DOFR}|$ varied from 0.55 mg km^{-1} to 45.94 mg km^{-1} with the mean of 10.18 mg km^{-1}. The PAM-OFR produced higher EFs in 26 out of the total 34 cycles, which was not expected based on a previous study

https://doi.org/10.5194/egusphere-2026-224
Preprint. Discussion started: 5 March 2026

where DOFR slightly exceeded PAM-OFR EFs (Simonen et al., 2024). The Pearson correlation coefficient R was 0.738, implying a strong correlation between the PAM-OFR and the DOFR EFs (Fig. 5b).

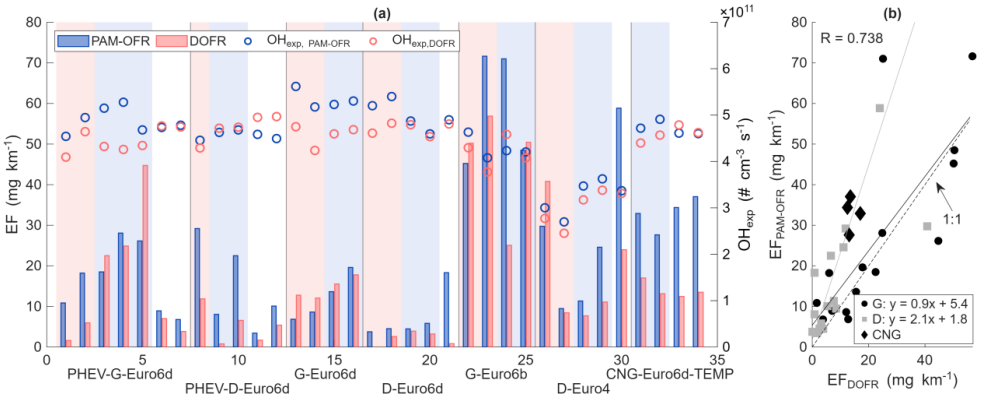

Figure 5. Secondary particle mass EFs (a) for all cycles. The cycles are grouped by vehicle and the cycle indexes on the x-axis correspond to Table S2. The mass concentrations measured by ELPI+ were corrected for DR, standard temperature, background concentration and particle losses on OFR walls. Parking was not included in the EF calculation. Average OH exposure (Eq. 1) is presented on the right y-axis. Ambient temperatures of -9, +23 and +35°C are denoted with blue, white and red background, respectively. The correlation coefficient R between the PAM-OFR and the DOFR EFs (b) is calculated from all data, but separate linear fits are shown for gasoline (G) and diesel (D) car cycles. One outlier was excluded in diesel linear fit calculation, and no linear fit is presented for CNG car cycles due to few repetitions.

Interestingly, the combusted fuel seems to have affected the difference between the OFRs. The PAM-OFR produced higher EFs than the DOFR in all cycles measured with diesel cars (cycles 8-12, 17-21 and 26-30), except for one (cycle 26), and in all cycles measured with the CNG car (cycles 31-34). The diesel car cycles seem to follow a linear fit (Fig. 5b) with the equation $EF_{PAM-OFR} = 2.1\ EF_{DOFR} + 1.8$ and R_{diesel} of 0.904. While the CNG car cycles are not included in the fit due to few repetitions, they seem to align with the fit. With the gasoline cars (cycles 1-7, 13-16 and 22-25), the fit equation was $EF_{PAM-OFR} = 0.9\ EF_{DOFR} + 5.4$, but the data points were more scattered ($R_{gasoline}$ 0.767).

3.2.1 Modern diesel cars

For the modern diesel cars (PHEV-D-Euro 6d and D-Euro 6d), low SecA formation was expected: Karjalainen et al. (2019) stated that PM_{aged} concentrations from a DPF-equipped diesel engine were roughly equal to pure dilution air measurements with the PAM-OFR. Also Platt et al. (2017) and Gordon et al. (2014a) observed negligible SOA formation in smog chamber measurements. In the Hartikainen et al. (2023) environmental chamber study, the secondary EFs exceeded detection limits only during DPF regeneration and cold start experiments. This was explained with low SOA precursor emissions and negligible condensation sink (CS) due to extremely low primary particle emissions. While modern diesel cars produced low PN_{fresh} and PM_{fresh} also in this study (see Fig. 3c, f and Fig. S4b), a significantly higher fraction of LVOCs was condensed on particles in the PAM-OFR than in the DOFR (Fig. S2a, b). With the PHEV-D-Euro 6d car, the fraction of LVOCs condensing on particles was on average 0.06 for the DOFR and 0.85 for the PAM-OFR, excluding the DPF regeneration cycle. This implies that the CS was low in the DOFR but not in the PAM-OFR, even though ingoing particle concentration was the same for both OFRs.

https://doi.org/10.5194/egusphere-2026-224
Preprint. Discussion started: 5 March 2026

The LVOC fate model revealed that in the DOFR, τ_{cond} was 278–594 s for the PHEV-D-Euro 6d car (excluding the DPF regeneration cycle) and 148–1035 s for the D-Euro 6d car (Fig. S2c). τ_{cond} describes the time to reach equilibrium between the gas and the particle phase and is inversely proportional to CS (see Eq. S2). As the τ_{cond} significantly exceeded the mean residence time of the DOFR (41 s), increasing the CS in the DOFR would have increased SecA mass. However, decreasing the dilution before the DOFR would not have been possible without removing the ED, which would have diminished the atmospheric relevance of the dilution and comparability of the experiments. Fig. S4f shows constant particle formation at <20 nm size range in the PAM-OFR, even when the vehicle (PHEV-D-Euro 6d) was parked. These particles seem to have increased the CS allowing easier LVOC condensation to particle phase. Since particle formation continues when engine is turned off, the particles were likely formed from compounds released from the PAM-OFR walls. Therefore, wall interactions seem to have affected SecA formation processes in the PAM-OFR, partially explaining higher EFs compared to the DOFR.

3.2.2 Modern gasoline and CNG cars

Modern gasoline cars (PHEV-G-Euro 6d and G-Euro 6d) produced more SecA than their diesel counterparts, which was expected based on previous research (see e.g., Platt et al., 2017). With the G-Euro 6d car, the DOFR EFs exceeded the PAM-OFR EFs in three out of four cycles. As seen in Fig. 4, the SecA emissions of the G-Euro 6d car were high during cold start and highway driving as strong pulses. During the pulses, the DOFR PN concentrations were roughly an order of magnitude higher than with the PAM-OFR, also at particle sizes that are significant for particle mass. This is due to the lower residence time of the DOFR. τ_{cond} in the DOFR for the G-Euro 6d car was 12–37 s, which indicates no underestimation of DOFR EFs. With the PHEV-G-Euro 6d car, the differences seem to be connected to ambient temperature, which affects primary and fresh emissions. At +23˚C and +35˚C, PAM-OFR EFs exceeded DOFR EFs in all cycles, and at +35˚C the differences were especially high. The electric motor was used more at +23˚C and +35˚C (66.1 % and 78.6 %, respectively) compared to -9˚C (43.6 %), leading to lower fresh particle and SecA precursor emissions. These percentages were from cycles with comparable battery charge at the start of the cycle. As discussed above, with the two modern diesel cars, the release of particle precursors from the PAM-OFR walls affected SecA formation when the electric motor was used. In cycle 5 (-9˚C), the measurement was started with an empty battery, which led to more combustion engine startups (57) than in the other two -9˚C cycles (38 ± 1). As SecA emissions were high during cold start with the G-Euro 6d car and the DOFR could capture them better, the amount of combustion engine startups could explain the higher DOFR EF in cycle 5 compared to the PAM-OFR. In general, the results indicate that a narrower RTD is beneficial for measurements with modern gasoline cars at transient driving conditions.

The PAM-OFR EFs exceeded DOFR EFs consistently in all cycles measured with the CNG-Euro 6d-TEMP car. Time series analysis showed that PN_{fresh} emissions were highest at small particle sizes (~10 nm), which is supported by Alanen et al. (2015) study. The exceptions in our study were highway driving and the cold start of cycle 31, where particles up to 100 nm diameter were emitted. These align with car manufacturer's specifications on times when the car will use gasoline instead of CNG. In cycle 32, the ambient temperature was unstable and higher than intended (on average -4˚C instead of -9˚C), which explains the lower EFs compared to cycle 31. The time series of SecA showed that the peak concentrations during pulses were at a similar level for both OFRs, unlike with the G-Euro 6d car. However, the concentrations in the PAM-OFR did not decrease as fast as in the DOFR, due to the different residence times of the OFRs. There was also consistent small particle formation in the

https://doi.org/10.5194/egusphere-2026-224
Preprint. Discussion started: 5 March 2026

PAM-OFR, caused by particle precursor release from the walls. Based on the LVOC fate model (Fig. S2b, c), DOFR EFs were not underestimated: τ_{cond} was 15.2-27.9 s, which is below the DOFR residence time (41 s).

3.2.3 Other effects

The OH exposure likely did not cause major EF differences between the OFRs, because the OH exposures were close ($2.01 \cdot 10^9$–$1.02 \cdot 10^{11}$ molec. cm^{-3} s^{-1}, which corresponds to 0.02–0.79 d as the absolute difference between the OFRs). While there is a relationship between the SecA mass and the OH exposure (see e.g., Tkacik et al., 2014), there was no correlation between OH exposure difference and EF difference. Cycles 8, 9, 10, 21, 30, 34 and 35 with near identical average OH exposures still resulted in differing EFs. On the other hand, cycles 3, 4, 13-16 had the highest OH exposure differences between the PAM-OFR and the DOFR, but the EFs were still comparable. High NO_x and VOC emissions decrease the OH exposure, because they are consuming more OH and therefore less tracer (CO) is oxidized. An example of this was the D-Euro 4 car: the lower OH exposure was not the cause of the high EFs, but rather a consequence of the high NO_x emissions. NO_x and VOC emissions, and consequently OH exposure, vary with time, depending on the driving condition and vehicle speed (see e.g., Drozd et al., 2016; Wang et al., 2022). When investigating the SecA potential of exhaust during transient cycles, maintaining a constant OH exposure all the time is impossible, and in this case adjusting the OFR settings right before the cycle would have ruined the cold start. Also in the study by Simon et al. (2025), done with the PAM-OFR, the effect of OH exposure on aged exhaust particle mass was not significant.

Figure 5a also shows significant variability between the repetitions, which was not completely unexpected considering how complex the studied phenomena were. The variability could be caused by differences in SecA precursor or in fresh particle emissions. With the old cars (G-Euro 6b and D-Euro 4), variability between repetitions was high, even though the LVOC fate model or OH exposure did not indicate any uncertainty. Karjalainen et al. (2014) stated that the storage and release phenomena of sulfur and hydrocarbon compounds in the EAS might affect nucleation mode formation in fresh exhaust and, in principle, that kind of phenomena can affect also PM_{aged}. It is also possible that certain driving conditions or changes in the exhaust temperature might trigger a sudden release of SecA precursors. The history of the sampling lines and OFR walls but also the history of EAS and tailpipe surfaces can affect the observed concentrations of emitted compounds. It is important to note that this kind of storage-release phenomena can affect real-world emissions, i.e., they should not be considered measurement artefacts.

Even though the cycle was driven as identically as possible each time, modern vehicles have intelligent control systems, e.g., a start-stop-system in all of the studied cars except for the D-Euro 4. These systems are not guaranteed to behave in the same way in repeated measurements. In addition, a DPF regeneration occurred in the middle of cycle 8 for the PHEV-D-Euro 6d car and two minutes before the end of cycle 18 for the D-Euro 6d car, which drastically increased the PM_{fresh} and subsequently the PM_{aged} EF (see Fig. 3f). For the PHEVs, clear reasons for the variability were the differences in the driving mode and the initial state of charge of the battery. Here the driving modes are the different strategies the vehicle has for alternating between the electric motor and the combustion engine, for example preserving the state of charge of the battery by favoring the combustion engine. Even with the same driving mode and initial state of charge, there were differences between the PHEV cycles in terms of electric motor usage and in the number of times the combustion engine was started.

https://doi.org/10.5194/egusphere-2026-224
Preprint. Discussion started: 5 March 2026

3.3 Background concentrations

As seen in Fig. 4, the OFRs produced a notable number concentration of small particles when the vehicle was parked. During parking, the engine was turned off but the instrument flows were kept the same. The origin of the sample during parking is unclear, possibly air pulled through the exhaust system. Regulated emissions were measured after a constant volume sampler (CVS), so it is also possible that the PTD sampled CVS dilution air during parking. When fresh particle emissions were low, for example with the modern diesel cars, PHEVs and the CNG car, particles formed from precursors released from PAM-OFR walls seem to have affected the SecA formation processes (see observations from Fig. 5).

Small particle formation was observed also during separate background measurements, when only purified pressurized air was fed to the system. Background PM and PN concentrations are presented in Fig. 6. The average background particle mass (PM_{bg}) concentrations were 9.10 µg m^{-3} for the PAM-OFR and 0.36 µg m^{-3} for the DOFR. The respective particle number (PN_{bg}) concentrations were $1.90 \cdot 10^5$ # cm^{-3} and $1.64 \cdot 10^3$ # cm^{-3}. The DOFR produced less particle mass and two orders of magnitude lower particle number concentrations than the PAM-OFR. Explanations for the high variability of PM_{bg} concentrations are investigated in Table 2.

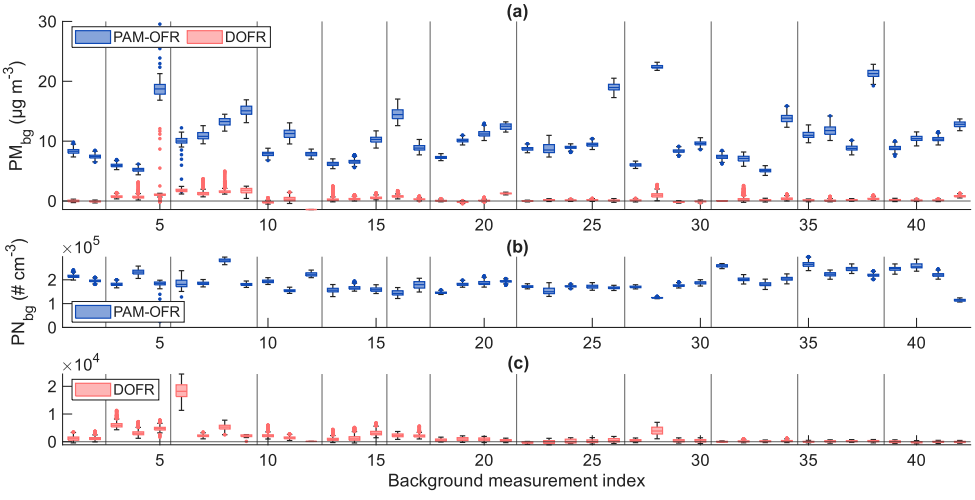

Figure 6. Background particle mass (a) and number (b, c) concentrations throughout the campaign. During background measurements, the system sampled purified pressurized air and the UV lights in the OFRs were on. Note the different scales in b and c. The vertical lines separate the measurement days and indicate OFR cleanings.

https://doi.org/10.5194/egusphere-2026-224
Preprint. Discussion started: 5 March 2026

Table 2. Correlation coefficients (R) between background PM concentrations and possible variables affecting them. They are classified as weak positive (0 < R < 0.3, indicated with +), moderate positive (0.3 < R < 0.7, ++), strong positive (0.7 < R < 1, +++) and weak negative (-0.3 < R < 0, -). Since the SP-AMS was always measuring after the PAM-OFR, correlations for sulfate (SO_4), nitrate (NO_3), ammonium (NH_4) and organics are not presented for the DOFR.

	PM_{bg} PAM-OFR	PM_{bg} DOFR
PM_{bg} (aged, PAM-OFR)	1	0.405 (++)
PM_{bg} (aged, DOFR)	0.405 (++)	1
$SO_{4,\,bg}$ (aged, PAM-OFR)	0.751 (+++)	N/A
$NO_{3,\,bg}$ (aged, PAM-OFR)	0.846 (+++)	N/A
$NH_{4,\,bg}$ (aged, PAM-OFR)	0.844 (+++)	N/A
Org_{bg} (aged, PAM-OFR)	0.847 (+++)	N/A
Emissions of the previously measured car		
PM (fresh)	0.120 (+)	0.330 (++)
BC (fresh)	0.254 (+)	0.414 (++)
PM (aged, DOFR)	N/A	0.659 (++)
PM (aged, PAM-OFR)	0.508 (++)	N/A
SO_4 (aged, PAM-OFR)	0.655 (++)	N/A
NO_3 (aged, PAM-OFR)	0.636 (++)	N/A
NH_4 (aged, PAM-OFR)	0.646 (++)	N/A
Org (aged, PAM-OFR)	0.776 (+++)	N/A
NO_x	0.315 (++)	0.461 (++)
NH_3	0.446 (++)	0.072 (+)
BTEX	0.071 (+)	-0.113 (-)

BTEX = benzene, toluene, ethylbenzene, xylenes

Unclean dilution air was likely not the source of the background PM produced in the OFRs, because of the relatively low correlation coefficient between the PAM-OFR and DOFR background PM (0.405). Also, the background concentrations of gaseous and particulate components in the dilution air were monitored and observed to be very low throughout the campaign. Instead, the emissions of the studied car seem to have had a significant effect on the background concentrations measured right after the cycle. Fresh PM, BC and NO_x emissions correlated moderately with the DOFR PM_{bg} and weakly with the PAM-OFR PM_{bg}. Highest DOFR backgrounds were measured mostly after the D-Euro 4, which produced soot particles and high fresh PM based on particle size distributions (see Fig. 3b, e), so this car could explain the correlations with fresh PM, BC and NO_x. On the other hand, fresh NH_3 and aged NH_4 emissions of the previously measured car correlated moderately with the PAM-OFR PM_{bg}. With the DOFR, there was no correlation with fresh NH_3, and aged NH_4 emissions after the DOFR were not measured. It seems that more NH_3, which is known to adsorb on surfaces easily, was deposited on the PAM-OFR than on the DOFR walls, leading to formation of NH_4NO_3 or $(NH_4)_2SO_4$ particles during background measurements. The PAM-OFR PM_{bg} correlated most strongly with organics out of all species measured by the SP-AMS during the driving cycle, but BTEX or other VOCs were not found to correlate with PM_{bg} from either of the OFRs. This indicates that there was background organic aerosol formation in the PAM-OFR, and that the BTEX were not important precursors to it. We want to note that this data does not allow comparison of the OFRs in this sense. For the PAM-OFR, there was a moderate correlation between time since last cleaning and PM_{bg},

https://doi.org/10.5194/egusphere-2026-224
Preprint. Discussion started: 5 March 2026

whereas for the DOFR, the correlation was weak. Moreover, Fig. 6 shows that on some days PAM-OFR PM_{bg} increased during the day while DOFR PM_{bg} stayed relatively stable, which supports the results from Table 2.

There are three ways to diminish the uncertainty caused by the background: 1) cleaning the OFR frequently, 2) subtracting the background concentrations or 3) decreasing dilution. However, all three options have challenges. Cleaning the OFRs is time-consuming as cleaning requires changing the UV intensity and possibly O_3 concentration. For this type of measurement with a relatively short driving cycle, it would have been possible to clean the OFRs between every cycle, but it would have meant a compromise in the total amount of cycles. In contrast, longer real driving or tunnel measurements do not have this possibility and the end of the measurement can be affected by the release of compounds from the OFR walls. Thus, monitoring the PM_{bg} between the measurements is important to estimate the necessary frequency and duration of the cleanings. The high time resolution combined with the possible instability of the high mass stages poses a challenge to the ELPI+ in PM_{bg} measurement. In principle, the SP-AMS and an SMPS (scanning mobility particle sizer) would suit the background monitoring better, but their relatively low time resolution is not ideal for measuring emissions during transient cycles or real driving.

Subtracting the baseline does not completely remove the background problem either, because for example particle size distributions can be of differing shapes during background and actual measurements. As seen in Fig. S4f, the background consists of a large number of small particles, but during the highway event the car produces larger particles. After the highway event the background particle production decreases for a while. Therefore, a simple subtraction may not work for PN or particle size distribution results. Out of online particle instruments, condensation particle counters (CPCs) are the most sensitive to OFR background, whereas the SP-AMS is one of the least sensitive because it has lower detection efficiency for particle sizes below 50 nm. It is important to note that background subtractions always introduce an error source to the results and might affect the comparability of different emission species.

Decreasing dilution before the OFR is also time-consuming during the campaign. Adjustable diluters might not be available, and the atmospheric relevance of the dilution might also limit the dilution adjustments. Opening the lines between measurements also increases the possibility of a leak in the sampling line, and adjusting dilution is always a risk in terms of repeatability of the measurements. This applies especially to OFR measurements, where concentrations of emission species affect the chemistry of SecA formation. Firstly, reaction rate always depends on the rate coefficient but also on reactant concentrations. As discussed for the DOFR, low fresh particle concentrations, i.e., too much dilution, did not allow equilibrium between gas and particle phase for the LVOCs, leading to potential underestimation of SecA. This can be a problem especially for modern diesel vehicles with DPFs. However, diesel vehicles also produce more NO_x than gasoline vehicles, and too high NO_x concentration consumes all OH radicals, potentially also leading to underestimation of SecA. Transient driving adds another layer of difficulty to adjusting dilution. As observed from Fig. 4 and other studies (Kuittinen et al., 2021; Simonen et al., 2019), cold starts produce a significant amount of SecA for gasoline cars, but TWC will decrease the concentrations as it warms up. Therefore, it is challenging to estimate a level of dilution that would be suitable for all parts of the driving cycle. Lastly, the detection limit of the instruments after the OFR is another thing to consider when adjusting dilution.

https://doi.org/10.5194/egusphere-2026-224
Preprint. Discussion started: 5 March 2026

During the measurement campaign, the background was monitored with ELPI+ and SP-AMS in frequent background measurements. The instruments chosen to measure aged aerosol were fit for the purpose, since a background subtraction was easy to do for PM concentrations. Adding SMPSs might have helped in background monitoring during the campaign, but otherwise they would have been unsuitable for the measurement. Dilution was not adjusted for each car as it would have risked comparability. For future measurements with modern diesel cars, we would seek ways to lower dilution, while keeping the dilution atmospherically relevant and NO_x concentrations low enough in the OFR. The OFRs were cleaned 1-2 times per day, and the results indicate that while the cleaning procedure seems to have been sufficient for the DOFR, the PAM-OFR would have benefited from more frequent cleaning.

4 Conclusions

SecA formation from passenger cars was studied with the PAM-OFR and the DOFR, which were assembled in parallel. Particle number and mass size distributions were comparable between the OFRs. SecA mass EFs were also correlated with a Pearson correlation coefficient of 0.738. While the PAM-OFR produced higher SecA mass EFs than the DOFR on average (22.90 mg km^{-1} and 15.77 mg km^{-1}, respectively), combusted fuel seems to have affected the EF differences between the OFRs. With gasoline cars, fast bursts of SecA formation during cold start and highway driving were captured more clearly by the DOFR, which led to DOFR EFs exceeding PAM-OFR EFs. However, whenever fresh PM emissions were very low, like with modern diesel cars, the CNG car or PHEVs, the SecA mass EFs were higher from the PAM-OFR than from the DOFR. The PAM-OFR produced small (<20 nm) particles consistently even when the vehicles were parked, and these particles seem to have increased the condensation sink for LVOCs. The EF difference was not caused by different OH exposures in the OFRs, and no effect of OH exposures on EFs was observed with this small range of OH exposures. All EF differences could not be explained by OFR characteristics, especially with the older cars, due to the complexity of the measurement setup and phenomena studied.

On average, the PAM-OFR produced more background PM (9.10 µg m^{-3}) than the DOFR (0.36 µg m^{-3}) and background PN ($1.90 \cdot 10^5$ and $1.64 \cdot 10^3$ # cm^{-3}, respectively) from purified pressurized air. PAM-OFR background concentrations were linked to emissions of the previously measured car, indicating greater wall losses compared to the DOFR. Despite subtracting background PM in EF calculation and cleaning both OFRs 1-2 times per day, particle precursor compounds released from PAM-OFR walls affected the SecA formation. For future OFR measurements with low emission cars, we would seek lower dilution before the OFR while still considering atmospheric relevance of the dilution and low NO_x concentrations in the OFR. Generally, paying attention to accurate and frequent background monitoring with suitable instruments and purified air is important.

While the two OFRs produced comparable results in terms of particle size distributions and SecA emission factors, the narrower residence time distribution and lower wall losses of the DOFR were beneficial qualities for transient vehicle emissions testing. In general, OFRs are valuable tools when investigating secondary particle formation and evaluating the total air quality impact of vehicle exhaust emissions. Still, existing emission regulation and mitigation technologies both target only the primary exhaust particle emissions from cars. In order to implement OFRs in regulatory emission testing and monitoring, further research and development as well as standardization of methodologies is needed.

https://doi.org/10.5194/egusphere-2026-224
Preprint. Discussion started: 5 March 2026

Data availability

Data is available upon request.

Author contribution

KK: Investigation, Formal analysis, Visualization, Writing – original draft preparation; MJ: Investigation, Formal analysis, Writing – review & editing; LS: Investigation, Formal analysis, Writing – review & editing; WH: Conceptualization, Investigation, Methodology, Project administration, Writing – review & editing; PM: Conceptualization, Methodology, Writing – review & editing; LS: Investigation, Writing – review & editing; TL: Investigation, Writing – review & editing; HL: Investigation, Writing – review & editing; LB: Conceptualization, Investigation, Writing – review & editing; HK: Investigation, Writing – review & editing; MR: Investigation, Supervision, Writing – review & editing; PB: Conceptualization, Funding acquisition, Resources; HT: Conceptualization, Funding acquisition, Project administration, Supervision, Writing – review & editing; PAS: Conceptualization, Funding acquisition, Project administration, Supervision, Writing – review & editing; TR: Conceptualization, Funding acquisition, Project administration, Supervision, Writing – review & editing;

Competing interest

The authors declare that they have no conflict of interest.

Acknowledgements

We acknowledge Dekati for providing the DOFR and a CO analyzer for the measurement campaign, as well as the support from Anssi Arffman. We thank Lassi Markkula from Tampere University, Delun Li, Minna Aurela, Sanna Saarikoski from FMI, and Anssi Järvinen from VTT for participation in the measurement campaign. In addition, collaboration with Jan Topinka, Tereza Červená and Michal Vojtíšek-Lom from IEM CAS is acknowledged.

Financial support

This work was supported by the European Union's Horizon Europe research and innovation programme under grant agreement No 101096133 (PAREMPI: particle emission prevention and impact: from real-world emissions of traffic to secondary PM of urban air).

References

Aerodyne Research. PAM users manual: https://pamusersmanual.jimdofree.com/protected/?comeFrom=https%3A%2F%2Fpamusersmanual.jimdofree.com%2Fpam-chem%2F&, last access 10 December 2025.

Alanen, J., Saukko, E., Lehtoranta, K., Murtonen, T., Timonen, H., Hillamo, R., Karjalainen, P., Kuuluvainen, H., Harra, J., Keskinen, J., Rönkkö, T.: The formation and physical properties of the particle emissions from a natural gas engine. Fuel, 162, 155–161, https://doi.org/10.1016/j.fuel.2015.09.003, 2015.

Alanen, J., Simonen, P., Saarikoski, S., Timonen, H., Kangasniemi, O., Saukko, E., Hillamo, R., Lehtoranta, K., Murtonen, T., Vesala, H., Keskinen, J., and Rönkkö, T.: Comparison of primary and secondary particle formation

https://doi.org/10.5194/egusphere-2026-224
Preprint. Discussion started: 5 March 2026

from natural gas engine exhaust and of their volatility characteristics. Atmos. Chem. Phys., 17, 8739–8755, https://doi.org/10.5194/acp-17-8739-2017, 2017.

Bruns, EA., El Haddad, I., Keller, A., Klein, F., Kumar, N. K., Pieber, S. M., Corbin, J. C., Slowik, J. G., Brune, W. H., Baltensperger, U., and Prévôt, A. S. H.: Inter-comparison of laboratory smog chamber and flow reactor systems on organic aerosol yield and composition. Atmos. Meas. Tech., 8, 2315–2332, https://doi.org/10.5194/amt-8-2315-2015, 2015.

Cohen, A. J., Brauer, M., Burnett, R., Anderson, H. R., Frostad, J., Estep, K., Balakrishnan, K., Brunekreef, B., Dandona, L., Dandona, R., Feigin, V., Freedman, G., Hubbell, B., Jobling, A., Kan, H., Knibbs, L., Liu, Y., Martin, R., Morawska, L., Pope, C. A. III, Shin, H., Straif, K., Shaddick, G., Thomas, M., van Dingenen, R., van Donkelaar, A., Vos, T., Murray, C. J. L., and Forouzanfar, M. H.: Estimates and 25-year trends of the global burden of disease attributable to ambient air pollution: an analysis of data from the Global Burden of Diseases Study 2015. The Lancet, 389, 1907-1918, https://doi.org/10.1016/S0140-6736(17)30505-6, 2017.

Daellenbach, K.R., Uzu, G., Jiang, J., Cassagnes, L.-E., Leni, Z., Vlachou, A., Stefenelli, G., Canonaco, F., Weber, S., Segers, A., Kuenen, J. J. P., Schaap, M., Favez, O., Albinet, A., Aksoyoglu, S., Dommen, J., Baltensperger, U., Geiser, M., El Haddad, I., Jaffrezo, J.-L., and Prévôt, A. S. H.: Sources of particulate-matter air pollution and its oxidative potential in Europe. Nature, 587, 414–419, https://doi.org/10.1038/s41586-020-2902-8, 2020.

Delaval, M., Czech, H., Almasaleekh, M., Offer, S., Pantzke, J., Ihalainen, M., Yli-Pirilä, P., Somero, M., Kortelainen, M., Gawlitta, N., Orasche. J., Jakobi, G., Shukla, D., Martens, P., Paul, A., Fang, Z., Pardo, M., Barth, A., Utinger, B., Jeong, S., Rastak, N., Kuhn, E., Huber, A., Mukherjee, A., Mesceriakovas, A., Joutsensaari, J., Leskinen, J., Hartikainen, A., Passig, J., Oeder, S., Schnelle-Kreis, J., Hohaus, T., Kiendler-Scharr, A., Kalberer, M., Di Bucchianico, S., Rudich, Y., Sippula, O., and Zimmermann, R.: The efficiency of EURO 6d car particulate filters is compromised by atmospheric aging: In vitro toxicity of gasoline car exhaust. Sci. Adv., 11, https://doi.org/10.1126/sciadv.adq2348, 2025.

Drozd, G. T., Zhao, Y., Saliba, G., Frodin, B., Maddox, C., Weber, R. J., Chang, M.-C.O., Maldonado, H., Sardar, S., Robinson, A. L., Goldstein, A. H.: Time Resolved Measurements of Speciated Tailpipe Emissions from Motor Vehicles: Trends with Emission Control Technology, Cold Start Effects, and Speciation. Environ. Sci. Technol., 50, 13592–13599, https://doi.org/10.1021/acs.est.6b04513, 2016.

EEA, European Environment Agency. Air pollutant emissions data viewer (Gothenburg Protocol, Air Convention) 1990-2023: https://www.eea.europa.eu/en/topics/in-depth/air-pollution/air-pollutant-emissions-data-viewer-1990-2023, last access 1 September 2025.

Fiore, A. M., Mickley, L. J., Zhu, Q., Baublitz, C. B.: Climate and Tropospheric Oxidizing Capacity. Annu. Rev. Earth Planet. Sci., 52, 321–349, https://doi.org/10.1146/annurev-earth-032320-090307, 2024.

Gordon, T. D., Presto, A. A., May, A. A., Nguyen, N. T., Lipsky, E. M., Donahue, N. M., Gutierrez, A., Zhang, M., Maddox, C., Rieger, P., Chattopadhyay, S., Maldonado, H., Maricq, M. M., and Robinson, A. L.: Secondary organic aerosol formation exceeds primary particulate matter emissions for light-duty gasoline vehicles. Atmos. Chem. Phys., 14, 4661–4678, https://doi.org/10.5194/acp-14-4661-2014, 2014a.

https://doi.org/10.5194/egusphere-2026-224
Preprint. Discussion started: 5 March 2026

Gordon, T. D., Presto, A. A., Nguyen, N. T., Robertson, W. H., Na, K., Sahay, K. N., Zhang, M., Maddox, C., Rieger, P., Chattopadhyay, S., Maldonado, H., Maricq, M. M., and Robinson, A. L.: Secondary organic aerosol production from diesel vehicle exhaust: impact of aftertreatment, fuel chemistry and driving cycle, Atmos. Chem. Phys., 14, 4643–4659, https://doi.org/10.5194/acp-14-4643-2014, 2014b.

Hartikainen, A., Ihalainen M., Yli-Pirilä, P., Hao, L., Kortelainen, M., Pieber, S. M., and Sippula, O.: Photochemical transformation and secondary aerosol formation potential of Euro6 gasoline and diesel passenger car exhaust emissions. J. Aerosol Sci., 171, 106159, https://doi.org/10.1016/j.jaerosci.2023.106159, 2023.

Ihalainen, M., Tiitta, P., Czech, H., Yli-Pirilä, P., Hartikainen, A., Kortelainen, M., Tissari, J.,Stengel, B., Sklorz, M., Suhonen, H., Lamberg, H., Leskinen, A., Kiendler-Scharr, A., Harndof, H., Zimmermann, R., Jokiniemi, J., and Sippula, O.: A novel high-volume Photochemical Emission Aging flow tube Reactor (PEAR). Aerosol Sci. Technol., 53, 276–294, https://doi.org/10.1080/02786826.2018.1559918, 2018.

Jathar, S.H., Friedman, B., Galang, A.A., Link, M.F., Brophy, P., Volckens, J., Eluri, S., Farmer D.K.: Linking load, fuel, and emission controls to photochemical production of secondary organic aerosol from a diesel engine. Environ. Sci. Technol., 51, 1377–1386, https://doi.org/10.1021/acs.est.6b04602, 2017.

Järvinen, A., Aitomaa, M., Rostedt, A., Keskinen, J., and Yli-Ojanperä, J.: Calibration of the new electrical low pressure impactor (ELPI+). J. Aerosol Sci., 69, 150–159, https://doi.org/10.1016/j.jaerosci.2013.12.006, 2014.

Kang, E., Root, M. J., Toohey, D. W., and Brune, W. H.: Introducing the concept of Potential Aerosol Mass (PAM). Atmos. Chem. Phys., 7, 5727–5744, https://doi.org/10.5194/acp-7-5727-2007, 2007.

Karjalainen, P., Rönkkö, T., Pirjola, L., Heikkilä, J., Happonen, M., Arnold, F., Rothe, D., Bielaczyc, P., and Keskinen, J.: Sulfur Driven Nucleation Mode Formation in Diesel Exhaust under Transient Driving Conditions. Environ. Sci. Technol., 48, 2336–2343, https://doi.org/10.1021/es405009g, 2014.

Karjalainen, P., Timonen, H., Saukko, E., Kuuluvainen, H., Saarikoski, S., Aakko-Saksa, P., Murtonen, T., Bloss, M., Dal Maso, M., Simonen, P., Ahlberg, E., Svenningsson, B., Brune, W. H., Hillamo, R., Keskinen, J., and Rönkkö, T.: Time-resolved characterization of primary particle emissions and secondary particle formation from a modern gasoline passenger car. Atmos. Chem. Phys., 16, 8559–8570, https://doi.org/10.5194/acp-16-8559-2016, 2016.

Karjalainen, P., Rönkkö, T., Simonen, P., Ntziachristos,L., Juuti, P., Timonen, H., Teinilä, K., Saarikoski, S., Saveljeff, H., Lauren, M., Happonen, M., Matilainen, P., Maunula, T., Nuottimäki, J., and Keskinen, J.: Strategies To Diminish the Emissions of Particles and Secondary Aerosol Formation from Diesel Engines. Environ. Sci. Technol., 53, 10408–10416, https://doi.org/10.1021/acs.est.9b04073, 2019.

Keskinen, J., Pietarinen, K., Lehtimäki, M.: Electrical low pressure impactor. J. Aerosol Sci., 23, 353–360, https://doi.org/10.1016/0021-8502(92)90004-F, 1992.

Keskinen, J. and Rönkkö, T.: Can Real-World Diesel Exhaust Particle Size Distribution be Reproduced in the Laboratory? A Critical Review. J. Air Waste Manag. Assoc., 60, 1245–1255, https://doi.org/10.3155/1047-3289.60.10.1245, 2010.

https://doi.org/10.5194/egusphere-2026-224
Preprint. Discussion started: 5 March 2026

Krechmer, J., Lopez-Hilfiker, F., Koss, A., Hutterli, M., Stoermer, C., Deming, B., Kimmel, J., Warneke, C., Holzinger, R., Jayne, J., Worsnop, D., Fuhrer, K., Gonin, M., and de Gouw, J.: Evaluation of a New Reagent-Ion Source and Focusing Ion–Molecule Reactor for Use in Proton-Transfer-Reaction Mass Spectrometry. Anal. Chem., 90, 12011–12018, https://doi.org/10.1021/acs.analchem.8b02641, 2018.

Kuittinen, N., McCaffery, C., Peng, W., Zimmerman, S., Roth, P., Simonen, P., Karjalainen, P., Keskinen, J., Cocker, D., Durbin, T., Rönkkö, T., Bahreini, R. & Karavalakis, G.: Effects of driving conditions on secondary aerosol formation from a GDI vehicle using an oxidation flow reactor. Environ. Pollut., 282, 117069, https://doi.org/10.1016/j.envpol.2021.117069, 2021.

Lambe, A. T., Ahern, A. T., Williams, L. R., Slowik, J. G., Wong, J. P. S., Abbatt, J. P. D., Brune, W. H., Ng, N. L., Wright, J. P., Croasdale, D. R., Worsnop, D. R., Davidovits, P., and Onasch, T. B.: Characterization of aerosol photo-oxidation flow reactors: heterogeneous oxidation, secondary organic aerosol formation and cloud condensation nuclei activity measurements. Atmos. Meas. Tech., 4, 445–461, https://doi.org/10.5194/amt-4-445-2011, 2011.

Lambe, A. T., Chhabra, P. S., Onasch, T. B., Brune, W. H., Hunter, J. F., Kroll, J. H., Cummings, M. J., Brogan, J. F., Parmar, Y., Worsnop, D. R., Kolb, C. E., and Davidovits, P.: Effect of oxidant concentration, exposure time, and seed particles on secondary organic aerosol chemical composition and yield, Atmos. Chem. Phys., 15, 3063–3075, https://doi.org/10.5194/acp-15-3063-2015, 2015.

Lee, SB., Bae, GN., Moon, KC.: Smog Chamber Measurements, in: Atmospheric and Biological Environmental Monitoring, edited by: Kim, Y.J., Platt, U., Gu, M.B., Iwahashi, H., Springer, 105–136 https://doi.org/10.1007/978-1-4020-9674-7_8, 2009.

Li, R., Palm, B. B., Ortega, A. M., Hlywiak, J., Hu, W., Peng, Z., Day, D. A., Knote, C., Brune, W. H., de Gouw, J. A., and Jimenez, J. L.: Modeling the Radical Chemistry in an Oxidation Flow Reactor: Radical Formation and Recycling, Sensitivities, and the OH Exposure Estimation Equation, J. Phys. Chem. A, 119, 4418–4432, https://doi.org/10.1021/jp509534k, 2015.

Li, K., Liggio, J., Lee, P., Han, C., Liu, Q., and Li, S.-M.: Secondary organic aerosol formation from α-pinene, alkanes, and oil-sands-related precursors in a new oxidation flow reactor, Atmos. Chem. Phys., 19, 9715–9731, https://doi.org/10.5194/acp-19-9715-2019, 2019.

Li, K., Zhang, J., Bell, D. M., Wang, T., Lamkaddam, H., Cui, T., Qi, L., Surdu, M., Wang, D., Du, L., El Haddad, I., Slowik, J. G., and Prevot, A. S. H.: Uncovering the dominant contribution of intermediate volatility compounds in secondary organic aerosol formation from biomass-burning emissions, Natl. Sci. Rev., 11, https://doi.org/10.1093/nsr/nwae014, 2024.

Mao, J., Ren, X., Brune, W. H., Olson, J. R., Crawford, J. H., Fried, A., Huey, L. G., Cohen, R. C., Heikes, B., Singh, H. B., Blake, D. R., Sachse, G. W., Diskin, G. S., Hall, S. R., and Shetter, R. E.: Airborne measurement of OH reactivity during INTEX-B, Atmos. Chem. Phys., 9, 163–173, https://doi.org/10.5194/acp-9-163-2009, 2009.

https://doi.org/10.5194/egusphere-2026-224
Preprint. Discussion started: 5 March 2026

Onasch, T. B., Trimborn, A., Fortner, E. C., Jayne, J. T., Kok, G. L., Williams, L. R., Davidovits, P., and Worsnop, D. R.: Soot Particle Aerosol Mass Spectrometer: Development, Validation, and Initial Application, Aerosol Sci. Technol., 46, 804–817, https://doi.org/10.1080/02786826.2012.663948, 2012.

Palm, B. B., Campuzano-Jost, P., Ortega, A. M., Day, D. A., Kaser, L., Jud, W., Karl, T., Hansel, A., Hunter, J. F., Cross, E. S., Kroll, J. H., Peng, Z., Brune, W. H., and Jimenez, J. L.: In situ secondary organic aerosol formation from ambient pine forest air using an oxidation flow reactor, Atmos. Chem. Phys., 16, 2943–2970, https://doi.org/10.5194/acp-16-2943-2016, 2016.

Park, M., Joo, H.S., Lee, K., Jang, M., Kim, S., Kim, I., Borlaza, L., Heungbin, L., Shin, H., Chung, K., Choi, Y.-H., Park, S., Bae, M.-S., Lee, J., Song, H., Park, K.: Differential toxicities of fine particulate matters from various sources. Sci. Rep., 8, 17007. https://doi.org/10.1038/s41598-018-35398-0, 2018.

Paul, A., Fang, Z., Martens, P., Mukherjee, A., Jakobi, G., Ihalainen, M., Kortelainen, M., Somero, M., Yli-Pirilä, P., Hohaus, T., Czech, H., Kalberer, M., Sippula, O., Rudich, Y., Zimmermann, R. and Kiendler-Scharr, A.: "Formation of Secondary Aerosol from Emissions of a Euro 6d-Compliant Gasoline Vehicle with a Particle Filter." Environ. Sci.: Atmos., 4, 802–812, https://doi.org/10.1039/d3ea00165b, 2024.

Peng, Z. and Jimenez, J. L.: Radical chemistry in oxidation flow reactors for atmospheric chemistry research. Chem. Soc. Rev., 49, 2570–2616, https://doi.org/10.1039/C9CS00766K, 2020.

Pieber, S. M., Kumar, N. K., Klein, F., Comte, P., Bhattu, D., Dommen, J., Bruns, E. A., Kılıç, D., El Haddad, I., Keller, A., Czerwinski, J., Heeb, N., Baltensperger, U., Slowik, J. G., and Prévôt, A. S. H.: Gas-phase composition and secondary organic aerosol formation from standard and particle filter-retrofitted gasoline direct injection vehicles investigated in a batch and flow reactor. Atmos. Chem. Phys., 18, 9929–9954, https://doi.org/10.5194/acp-18-9929-2018, 2018.

Platt, S.M., El Haddad, I., Pieber, S.M., Zardini, A. A., Suarez-Bertoa, R., Clairotte, M., Daellenbach, K. R., Huang, R.-J., Slowik, J. G., Hellebust, S., Temime-Roussel, B., Marchand, N., Gouw, J. de, Jimenez, J. L., Hayes, P. L., Robinson, A. L., Baltensperger, U., Astorga, C. & Prévôt, A. S. H.: Gasoline cars produce more carbonaceous particulate matter than modern filter-equipped diesel cars. Sci. Rep., 7, 4926, https://doi.org/10.1038/s41598-017-03714-9, 2017.

Rönkkö, T., Virtanen A., Vaaraslahti, K., Keskinen, J., Pirjola, L., and Lappi, M.: Effect of dilution conditions and driving parameters on nucleation mode particles in diesel exhaust: Laboratory and on-road study. Atmos. Environ., 40, 2893–2901, https://doi.org/10.1016/j.atmosenv.2006.01.002, 2006.

Timonen, H., Karjalainen, P., Saukko, E., Saarikoski, S., Aakko-Saksa, P., Simonen, P., Murtonen, T., Dal Maso, M., Kuuluvainen, H., Bloss, M., Ahlberg, E., Svenningsson, B., Pagels, J., Brune, W. H., Keskinen, J., Worsnop, D. R., Hillamo, R., and Rönkkö, T.: Influence of fuel ethanol content on primary emissions and secondary aerosol formation potential for a modern flex-fuel gasoline vehicle. Atmos. Chem. Phys., 17, 5311–5329, https://doi.org/10.5194/acp-17-5311-2017, 2017.

Tkacik, D., Lambe, A. T., Jathar, S., Li, X., Presto, A. A., Zhao, Y., Blake, D., Meinhardi, S., Jayne, J. T., Croteau, P. L., and Robinson, A. L.: Secondary Organic Aerosol Formation from in-Use Motor Vehicle Emissions Using a

https://doi.org/10.5194/egusphere-2026-224
Preprint. Discussion started: 5 March 2026

Potential Aerosol Mass Reactor. Environ. Sci. Technol., 48, 11235–11242, https://doi.org/10.1021/es502239v, 2014.

Saarikoski, S., Järvinen, A., Markkula, L., Aurela, M., Kuittinen, N., Hoivala, J., Barreira, L.M.F., Aakko-Saksa, P., Lepistö, T., Marjanen, P., Timonen, H., Hakkarainen, H., Jalava, P., and Rönkkö, T.: Towards zero pollution vehicles by advanced fuels and exhaust aftertreatment technologies. Environ. Pollut., 347, 123665, https://doi.org/10.1016/j.envpol.2024.123665, 2024.

Shaw, J. T., Rickard, A. R., Newland, M. J., and Dillon, T. J.: Rate coefficients for reactions of OH with aromatic and aliphatic volatile organic compounds determined by the multivariate relative rate technique, Atmos. Chem. Phys., 20, 9725–9736, https://doi.org/10.5194/acp-20-9725-2020, 2020.

Simon, L., Barreira, L., Kylämäki, K., Saarikoski, S., Aurela, M., Li, D., Järvinen, A., Kuutti, H., Honkisz, W., Jäppi, M., Salo, L., Rissanen, M., Červená, T., Vojtíšek, M., Topinka, J., Bielaczyc, P., Rönkkö, T., Aakko-Saksa, P., and Timonen, H.: From Real-Driving Emissions to Urban Air Quality: Composition of Aged PM from Modern Diesel, Gasoline, and CNG Fueled Cars and Plug-in Hybrid Electric Vehicles. Atmos. Environ.: X, 28, 100375, https://doi.org/10.1016/j.aeaoa.2025.100375, 2025.

Simonen, P., Saukko, E., Karjalainen, P., Timonen, H., Bloss, M., Aakko-Saksa, P., Rönkkö, T., Keskinen, J., and Dal Maso, M.: A new oxidation flow reactor for measuring secondary aerosol formation of rapidly changing emission sources. Atmos. Meas. Tech., 10, 1519–1537, https://doi.org/10.5194/amt-10-1519-2017, 2017.

Simonen, P., Kalliokoski, J., Karjalainen, P., Rönkkö, T., Timonen, H., Saarikoski, S., Aurela, M., Bloss, M., Triantafyllopoulos, G., Kontses, A., Amanatidis, S., Dimaratos, A., Samaras, Z., Keskinen, J., Dal Maso, M., Ntziachristos, L.: Characterization of laboratory and real driving emissions of individual Euro 6 light-duty vehicles – Fresh particles and secondary aerosol formation. Environ. Pollut., 255, 113175, https://doi.org/10.1016/j.envpol.2019.113175, 2019.

Simonen, P., Dal Maso, M., Prauda, P., Hoilijoki, A., Karppinen, A., Matilainen, P., Karjalainen, P., and Keskinen, J.: Estimating errors in vehicle secondary aerosol production factors due to oxidation flow reactor response time. Atmos. Meas. Tech., 17, 3219–3236, https://doi.org/10.5194/amt-17-3219-2024, 2024.

Wang, S., Yuan, B., Wu, C., Wang, C., Li, T., He, X., Huangfu, Y., Qi, J., Li, X.-B., Sha, Q., Zhu, M., Lou, S., Wang, H., Karl, T., Graus, M., Yuan, Z., and Shao, M.: Oxygenated volatile organic compounds (VOCs) as significant but varied contributors to VOC emissions from vehicles, Atmos. Chem. Phys., 22, 9703–9720, https://doi.org/10.5194/acp-22-9703-2022, 2022.

Watne Å.K., Psichoudaki, M., Ljungström, E., Le Breton, M., Hallquist, M., Jerksjö, M., Fallgren, H., Jutterström, S., and Hallquist, Å.M.: Fresh and Oxidized Emissions from In-Use Transit Buses Running on Diesel, Biodiesel, and CNG. Environ. Sci. Technol., 52, 7720-7728, https://doi.org/10.1021/acs.est.8b01394, 2018.

Wu, C., Brown, R. A., Brown, Z. E., Trounce, H., Horchler, E. J., Wang, L., Miljevic, B., Zhang, C., Wang, H., Wang, B., Ristovski, Z., Stevanovi, S.: A New Oxidation Flow Reactor for the Measurements of Secondary Aerosol Formation: Characterisation and a Case Study. Atmos. Environ., 309, 119886, https://doi.org/10.1016/j.atmosenv.2023.119886, 2023.

https://doi.org/10.5194/egusphere-2026-224
Preprint. Discussion started: 5 March 2026

Xu, N. and Collins, D. R.: Design and characterization of a new oxidation flow reactor for laboratory and long-
745 term ambient studies, Atmos. Meas. Tech., 14, 2891–2906, https://doi.org/10.5194/amt-14-2891-2021, 2021.

Zhang, Z., Xu, W., Lambe, A. T., Hu, W., Liu, T., and Sun, Y.: Insights Into Formation and Aging of Secondary Organic Aerosol From Oxidation Flow Reactors: A Review. Curr. Pollut. Rep., 10, 387–400, https://doi.org/10.1007/s40726-024-00309-7, 2024.

Zhang, J., Peng, J., Song, A., Lv, Z., Tong, H., Du, Z., Guo, J., Wu, L., Wang, T., Hallquist, M. and Mao, H.:
750 Marked impacts of transient conditions on potential secondary organic aerosol production during rapid oxidation of gasoline exhausts. npj Clim. Atmos. Sci., 6, 59, https://doi.org/10.1038/s41612-023-00385-4, 2023.

Zhao, Y., Lambe, A. T., Saleh, R., Saliba, G., and Robinson, A.: Secondary Organic Aerosol Production from Gasoline Vehicle Exhaust: Effects of Engine Technology, Cold Start, and Emission Certification Standard. Environ. Sci. Technol., 52, 1253–1261, https://doi.org/10.1021/acs.est.7b05045, 2018.